

# Electrical manipulation of inter-valley trions in twisted MoSe<sub>2</sub> homobilayers at room temperature

Bárbara L. T. Rosa,<sup>1,\*</sup> Paulo E. Faria Junior,<sup>2</sup> Alisson R. Cadore,<sup>3</sup> Yuhui Yang,<sup>1</sup> Aris Koulas-Simos,<sup>1</sup> Chirag C. Palekar,<sup>1</sup> Sefaattin Tongay,<sup>4</sup> Jaroslav Fabian,<sup>2</sup> and Stephan Reitzenstein<sup>1</sup>

<sup>1</sup>*Institute of Solid State Physics, Technische Universität Berlin, 10623 Berlin, Germany*

<sup>2</sup>*Institute for Theoretical Physics, University of Regensburg, 93040 Regensburg, Germany*

<sup>3</sup>*Brazilian Nanotechnology National Laboratory, Brazilian Center for*

*Research in Energy and Materials, Campinas, Sao Paulo 13083-970, Brazil*

<sup>4</sup>*School for Engineering of Matter, Transport and Energy, Arizona State University, Tempe, USA*

The impressive physics and applications of intra- and interlayer excitons in a transition metal dichalcogenide twisted-bilayer make these systems compelling platforms for exploring the manipulation of their optoelectronic properties through electrical fields. This work studies the electrical control of excitons in twisted MoSe<sub>2</sub> homobilayer devices at room temperature. Gate-dependent micro-photoluminescence spectroscopy reveals an energy tunability of several meVs originating from the emission of excitonic complexes. Furthermore, it investigates the twist-angle dependence of valley properties by fabricating devices with distinct stacking angles. Strengthened by density functional theory calculations, the results suggest that, depending on the rotation angle, the conduction band minima and hybridized states at the **Q**-point promote the formation of inter-valley trions involving the **Q**- and **K**-points in the conduction band and the **K**-point in the valence band. Besides exploring the charge-carrier manipulation in twisted homobilayers, our findings open new avenues for engineering multifunctional optoelectronic devices based on ultrathin semiconducting systems.

## INTRODUCTION

Van der Waals heterostructures (vdWHs) based on stacked monolayers (MLs) of transition metal dichalcogenides (TMDs) have emerged as striking artificial semiconductor systems due to their unique characteristics driven by lattice mismatch effects [1–4]. The wide variability of the materials combined with the twist angle between the layers, lead to additional degrees of freedom that play a crucial role in the spin-valley dynamics of van der Waals systems [1–7] and their intra- and interlayer exciton complexes. While studies of TMD heterostructures have predominantly centered on vdWHs composed of different MLs, an intriguing avenue opens up in the exploration of twisted homobilayers (t-BLs). Those stacked layers of the same material with a controlled rotation angle potentially exhibit more pronounced spin-valley properties than heterobilayers, in which the absence of lattice mismatch can lead to the formation of hybridized states [3–5], reconstructed domains [3] and inter- and intralayer excitons trapped in moiré superlattices with a periodicity of tenths of nanometers [4, 5].

Exploring the electrostatic landscape of TMD-based vdWHs has also appeared as a potential avenue to fingerprint the twist-angle characteristics through exciton complexes photoluminescence response [3, 4, 8]. However, the small oscillator strength of interlayer excitons (IX) [9, 10] attributed to significant electron and hole separation in momentum and real spaces [1–4] has limited investigations mainly to their optical properties at cryogenic temperatures. Intralayer exciton, on the other hand, turns

out to be a promising platform to the study of optoelectronic properties in vdWHs, even at room temperature (RT), due to their strong oscillator strength. Moreover, previous reports suggest that t-BLs present significant measurable variations in the intralayer excitons [5, 6], a result weakly observed in heterobilayers due to the suppression of their intralayer optical response of at least one layered material [2, 7].

In this work, we report the ability to control exciton complexes in MoSe<sub>2</sub> homobilayers through gated micro-photoluminescence ( $\mu$ PL) spectroscopy at RT. By varying the twist angle ( $\theta$ ) between the MoSe<sub>2</sub> MLs, we observe an angle-rotation-dependent modulation of the charge-carrier concentration, strongly impacting both neutral and charged (trions) intralayer excitons. At R-type stacking configuration of  $\theta \sim 1^\circ$ , the t-BL exhibits an intrinsic *n*-type doping behaviour that efficiently enhances an exciton-to-trion conversion by electrostatic doping. Conversely, the large angle mismatch of the t-BL with  $\theta \sim 18^\circ$  presents a close to charge-neutrality character, in which the neutral exciton features the main emission response independently of the applied bias. Density functional theory (DFT) calculations predict the existence of a conduction band minimum (CBM) located in the **Q**-point of the Brillouin zone instead of **K**/**K'**-points [11, 12] as expected for TMD MLs, in addition to hybridized states at **Q**-point. Therefore, we explain our experimental results considering that photo-excited electrons are transferred to **Q**- and **K**-points after photon absorption, inducing charged-excitons emission through inter-valley trions formation. On the other hand, large twist angles experience no trionic enhancement, mainly due to the reduction of interlayer coupling strength effects. The findings herein provide new insights into the externally controlled optoelectronic characteris-

\* rosa@physik.tu-berlin.de

tics of TMD-based vdWHs at RT, promoting the development and solid applicability of layered semiconducting material devices.

## EXPERIMENTAL RESULTS AND DISCUSSION

We fabricated artificially stacked MoSe<sub>2</sub> homobilayers using the tear-and-stack technique [13], as described in the Methods section. A schematic figure of the device structure is seen in Figure 1a. The experiments were performed on three samples with  $\theta = (1 \pm 1)^\circ$ ,  $(4 \pm 1)^\circ$  and  $(18 \pm 1)^\circ$ . The angle deviation was based on the equipment precision once the technique of tear-and-stick has been performed to achieve high-precision angles below  $1^\circ$ , as reported in the literature for superconductivity in magic-angle graphene superlattices[14] and similar works[3–5]. We decided for those specific angles to investigate the properties of small angles as well as the effects of large twist angles that still conserve R stacking properties (e.g., non spin-valley locking[5]) and interlayer coupling strength[5].

An optical image of sample  $\theta \sim 1^\circ$  is seen in Figure 1b.  $\mu$ PL and gate-dependent  $\mu$ PL spectra were recorded from ML and t-BL regions of every device, confirming that the MLs response of each sample is similar under the same experimental conditions and, therefore, reassuring that the distinct features observed in the t-BLs are predominantly related to the stacking configuration (e.g., different twist-angles). It is worth mentioning that in the present work, we limit the discussion to devices with  $\theta \sim 1^\circ$  and  $\sim 18^\circ$ , since the sample with  $\theta \sim 4^\circ$  presents similar results as  $\theta \sim 1^\circ$  (see Supporting Information, Sec.1).

We display in Figure 1c a simplified scheme of carrier transition mechanisms in TMD systems. Figures 1d–f compare the RT PL spectra at the intralayer emission range for devices with different twist angles, extracted from ML and t-BL regions under continuous-wave (CW) 660 nm laser excitation. We notice an asymmetric emission peak at the ML region (Figure 1d), which we assigned under double-Voigt fitting to a convolution of two peaks, the neutral exciton ( $X^0$ ) at  $\sim 1.56$  eV [15, 16] and an additional feature at lower energy ( $\sim 1.52$  eV) and weaker spectral weight (85% of  $X^0$ ). Considering the trionic binding energy between 25 to 43 meV (depending on the dielectric environment and measurement conditions) reported in the literature of TMD MLs[17–21], we assigned the peak at  $\sim 1.52$  eV to charged-exciton/trion ( $X^-$ ) emission. The PL emission of t-BL1 $^\circ$ , on the contrary, displays a comparable spectral weight between the two excitonic features  $X^0$  and  $X^-$ , as seen in Figure 1e, and a PL quenching of 20x compared to the ML emission. The observed response can be related to the efficient ultrafast interlayer carrier transfer between the MoSe<sub>2</sub> MLs after the dissociation of electrons and holes into separate layers[1, 3, 5]. Remarkably, the t-BL18 $^\circ$  device displays a behaviour neither noticed in the ML nor the t-BL1 $^\circ$  samples. Here, only one feature could be satisfactorily

fitted at approximately 1.545 eV, indicating a major contribution from one excitonic complex. Based on further discussion, this peak is associated with  $X^0$  emission. Additionally, it shows no decrease in PL-yield compared to the ML, a result attributed to the substantial reduction in interlayer coupling strength between the layered MLs, at which suppression of charger transfer between layers occurs due to the large  $\theta$  [5, 7]. The noticeable redshift emission of  $\sim 20$  meV in comparison with the ML has also been reported [5] and can be addressed to the dielectric screening as a consequence of an asymmetric stacking structure formed by the adjacent MoSe<sub>2</sub> layer and the h-BN layer[22, 23].

The origin of the charge carrier concentration on t-BLs is next investigated through gate voltage-dependent PL studies in a capacitor-like geometry, as illustrated in Figure 1a. Figures 2a–c show color plots of normalized PL emission as a function of the applied back gate voltage ( $V_g$ ) in which a distinct gate-dependent response from ML, t-BL1 $^\circ$  and t-BL18 $^\circ$  devices, respectively, is noticeable (the raw PL data can be seen in the Supporting Information, Sec. 2). For the ML and t-BL18 $^\circ$  regions, the dominant energy remains the ascribed  $X^0$  contribution ( $\sim 1.56$  eV and  $\sim 1.54$  eV in the case of ML and t-BL18 $^\circ$ , respectively), regardless of a slight peak broadening for  $V_g > 0$  (Figures 2a,c). The PL emission of t-BL1 $^\circ$  device, in contrast, shows a continuous change of energy from 1.56 to 1.52 eV together with a substantial linewidth dependence with  $V_g$ .

For better comparison, Figures 2d–f show the extracted gated-PL spectra for  $V_g = -1.6$  V, 0 V, and 1.6 V for ML, t-BL1 $^\circ$  and t-BL18 $^\circ$  devices, respectively. First analyzing the ML data (Figure 2d), we observe an asymmetric PL emission broadening towards positive  $V_g$ . As expected, in this device’s architecture,  $V_g$  establishes the charge modulation (e.g., electrostatic doping), and hence, the Fermi level ( $E_F$ ) shift within the material. As such, through an applied positive (negative) bias, electrons (holes) are driven into the MoSe<sub>2</sub> active material. The emission of a MoSe<sub>2</sub> ML at RT typically consists of a dominant feature ascribed to  $X^0$ . However, depending on the charge carrier concentration, the  $X^0/X^-$  ratio can be altered by introducing holes or electrons in the system. Considering the results displayed in Figures 2a,d, we note an intrinsic  $n$ -type doping nature of our crystal due to the trionic appearance only under positive  $V_g$ . Electrostatic doping effects seem to appear even stronger in the t-BL1 $^\circ$  device, where the overall excitonic emission is strongly tuned by just altering the charge doping, and thus, modulating what we ascribed as  $X^-$  response (see Figure 2e). The t-BL18 $^\circ$  device, on the contrary, exhibits a weak spectral weight variation (Figure 2f) as an explicit characteristic of intrinsic charge neutrality. Significant attention should be paid to the electrostatic doping effects observed in the three distinct devices. On collecting the gate-voltage-dependent PL, we extracted the emission intensities and the maximum peak energy and displayed the results in Figures 2g–i as a function

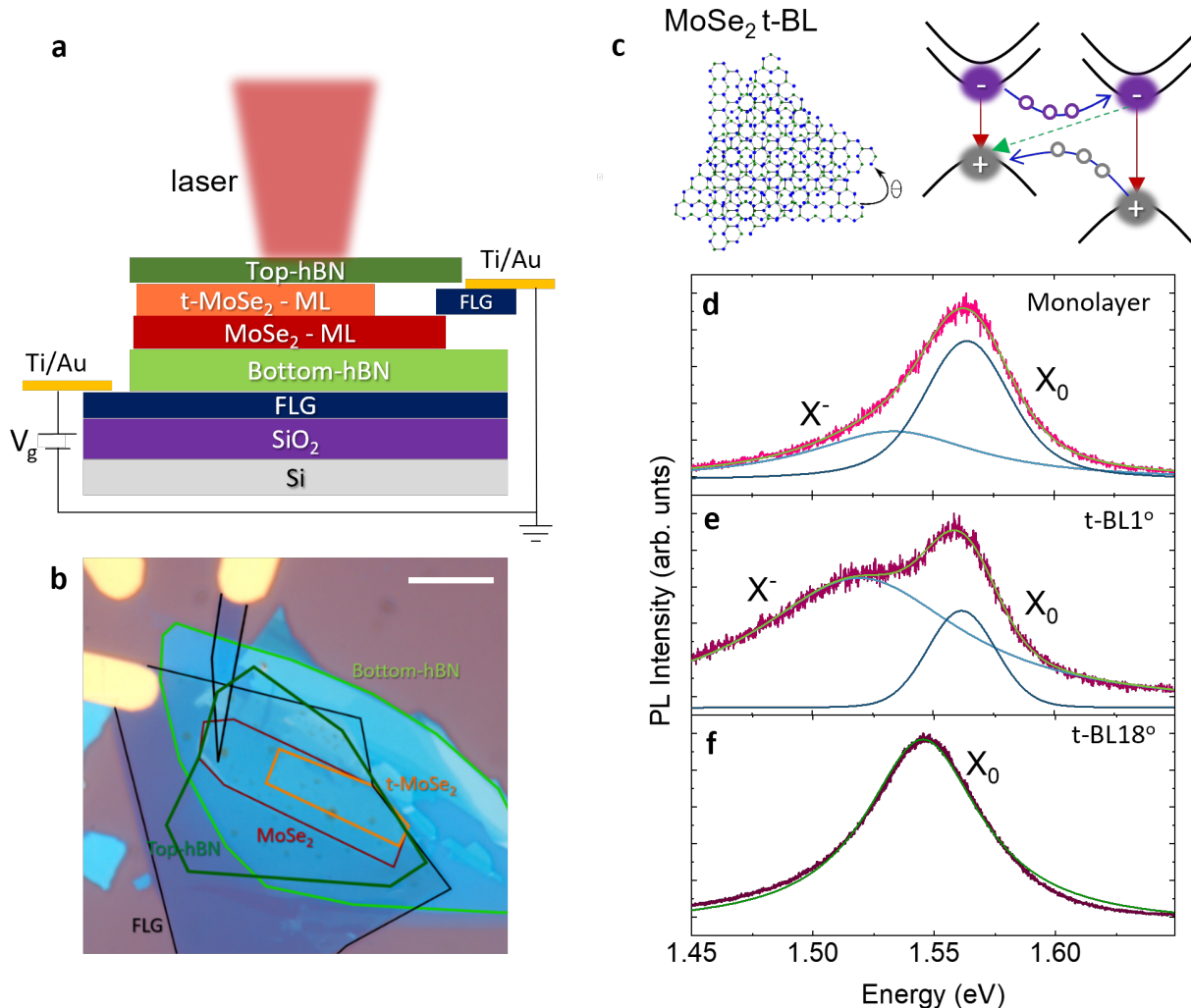


FIG. 1. **MoSe<sub>2</sub> t-BL device properties.** (a), Schematic structure of our gate-controlled t-BL device. (b) Optical image of a fabricated t-BL device. The scale var corresponds to  $10\mu\text{m}$ . (c) Lattice structure of a stacking twisted MoSe<sub>2</sub>/MoSe<sub>2</sub> homobilayer, and a simplified generic schematic of associated carrier transition mechanisms in the case of TMD hetero- or homobilayers. Red solid arrows, blue solid arrows, and green dashed arrows represent, respectively, the intralayer transition, the interlayer carrier transfer between the different MLs, and the IX exciton transition between the different MLs. PL emission of a ML, t-BL1° and t-BL18° (d-f) at RT, measured using a CW 660 nm laser. The average excitation power used in all measurements was  $10\mu\text{W}$ . In all figures, X<sup>0</sup> and X<sup>-</sup> represent the neutral exciton and trion emissions, respectively.

of  $V_g$ . We first notice a drastic PL intensity modulation in the three regions through the applied bias. As well-stated, electrostatic doping determines the carrier recombination process in an intrinsic  $n$ -type semiconductor, tuning between charge neutrality for  $V_g < 0$  to high carrier concentration for  $V_g > 0$  [17, 24–28].

Meanwhile, a high gate-induced doping level may not only provide the formation of charged excitons but promote nonradiative recombination processes[29] (e.g., trap-assisted recombination[29] or Auger recombination[17, 20, 24, 25, 29, 30]), responsible for reducing the PL yield drastically. As depicted in Figure 2g, although  $V_g$  sweeping alters the PL intensity, the dominant peak energy belongs to the X<sup>0</sup> emission. In contrast, the t-BL1° device region shows a strongly

gate-dependent PL under the same measurement conditions as the ML region, leading to a robust exciton-trion conversion mechanism as indicated in Figure 2h by the blue vertical arrow. Similar results have been reported for several heavily doped TMD ML devices (e.g., WS<sub>2</sub> MLs [19, 20, 25, 31, 32]). Our findings, however, suggest that the chosen twist-angle of the t-BL plays an essential role in charge carrier concentration of the system, as we further discuss with the help of theoretical calculations. It is worth mentioning that all t-BL devices were fabricated onto bottom hBN flakes of similar thickness ( $20\text{nm}$ ), therefore, the observed spectral changes cannot be associated to difference in induced charge carriers by  $V_g$ . Between  $V_g$  of  $-1.6\text{V}$  and  $-0.8\text{V}$  (Figure 2h), the t-BL1° device PL emission shows a dip observed over

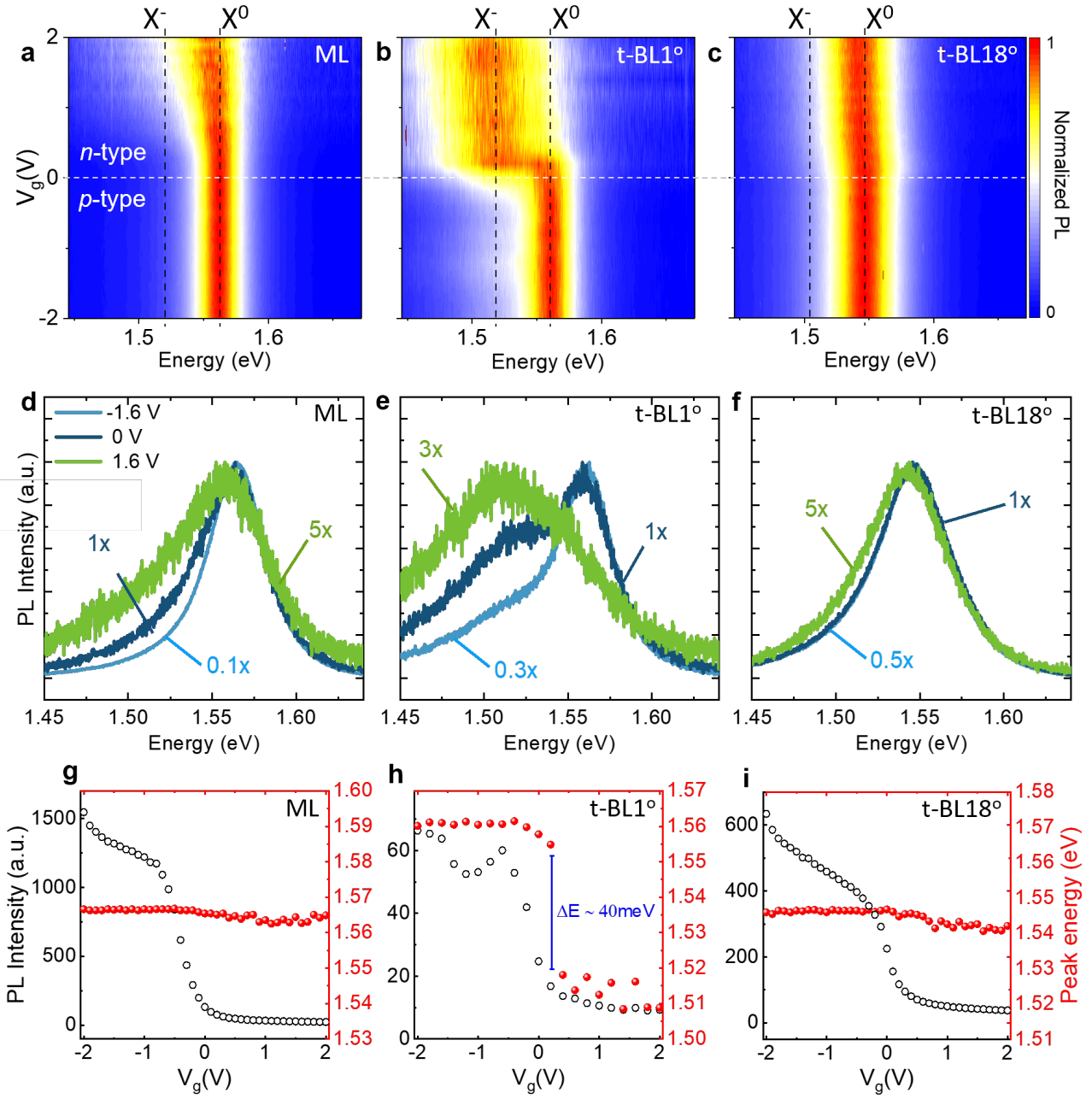


FIG. 2. **Gate-controlled PL modulation in MoSe<sub>2</sub> t-BLs devices.** The color plot of the PL spectra for (a) ML MoSe<sub>2</sub>, (b) t-BL1<sup>o</sup> and (c) t-BL18<sup>o</sup> devices as a function of the gate voltage ( $V_g$ ). The dashed white lines indicate the regions with  $p$ - and  $n$ -type doping behavior, while the expected energy position for  $X^0$  and  $X^-$  are indicated by dashed black lines. The PL intensity in the color plot was normalized for better comparison. The average excitation power used in all measurements was  $10\mu\text{W}$ . (d–f) Selected gated-PL spectra for ML MoSe<sub>2</sub>, t-BL1<sup>o</sup> and t-BL18<sup>o</sup> devices, respectively. The PL spectra were vertically shifted and the intensity was adjusted for better comparison. (g–i) Maximum PL intensity (left axis) and peak energy position (right axis) for the neutral exciton (red solid symbols) and trions (black empty symbols) in the ML MoSe<sub>2</sub>, t-BL1<sup>o</sup> and t-BL18<sup>o</sup> devices, respectively. The ML data displayed in (a) were extracted from t-BL1<sup>o</sup> device.

several applied-bias cycles. Till this date, we could not address a specific reason that might be altering the PL response of the t-BL1<sup>o</sup> device in this  $V_g$  range.

In Figure 2, we notice that at negative  $V_g$ , the t-BL1<sup>o</sup> device shows no saturation point upon the same values

applied to the ML and the t-BL1<sup>o</sup> regions. The overall scenario of the t-BL18<sup>o</sup> device resembles the ML result (Figure 2c), wherein the conversion of excitons into trions has not been observed up to the limit of our applied positive  $V_g$ . Such response indicates a weak interaction

between the MLs, likely caused by increased interlayer distance dependent on the twist angle [5, 7, 33]. However, one must not overlook the potential impact of ultrafast carrier scattering between the intra-band of adjacent layers (refer to Figure 1c), which can also disrupt the number of electron and hole carriers recombining radiatively in the same layer, ultimately decreasing the exciton emission. We highlight that, although this study presents a careful analysis regarding the exciton complexes behaviour in TMD stacking devices, further investigation applying different techniques may be needed to address in details the minor changes in the energy emission behaviour. The data regarding the ML region of sample t-BL18° presents similar response as for the ML region of t-BL1° (Figure S6).

To gain additional insight into the optical properties of our gate-controlled t-BLs, we performed DFT calculations to reveal the twist-angle-dependent characteristics of the different systems, such as the relevant band edges, band alignment, and interlayer coupling strength [33]. Further details about DFT calculation can be seen in Supplementary Information, Section 3. The selected configurations for the homobilayer systems are based on the energetically favourable stacking composition in the case of  $\theta = 0^\circ$  ( $R_h^M$ -stacking configuration), and the smallest structure closest to our experimental value of  $\theta \sim 18^\circ$ , which is  $\theta \sim 21.8^\circ$  (Figure 3a). In both configurations, the relevant band edges involved in the optical process discussed here are the CBM at **K**- and **Q**-points, and valence band maximum at **K**- and  $\Gamma$ -points. Particularly, our calculations show that the relative energy separation and interlayer hybridization of these different bands strongly depend on the twist angle, in line with other reports[3, 5]. Therefore, the observed intralayer PL-yield reduction of t-BL1° has been ascribed to the ultrafast photo-excited carrier transfer between the adjacent MLs, induced by the proximity between layers, and the hybridization of states, facilitating IX formation[3, 5]. On the contrary, t-BL18° is expected to decrease considerably the IX recombination since the large stacking angles alter the interlayer distance, consequently suppressing the interlayer transfer channels [5, 7]. However, this understanding lacks an additional explanation for the distinct carrier concentration observed in our systems.

The exciton manipulation through gate-voltage is explained in the case of our t-BLs considering the forming band structure after the layer stacking. Figure 3b schematizes the energy level diagrams of t-BL1° and t-BL18° (at  $V_g = 0$  V), based on our experimental and theoretical inputs. For the t-BL1° device, our theoretical analysis suggests that the CBM in the **Q**-point that lies at lowest energy, favours the electrons created by photon absorption and electrostatic doping to be pushed into that **Q**-point. Moreover, since it presents hybridized states (Figure 3b, in orange), we suggest the formation of trions composed by electrons in **Q**- and **K**-points bounded to holes in the **K**-point[11], as schematized in Figure 3b (t-BL1° case). This scenario indi-

cates a robust inter-valley trionic response in the t-BL1°, which, hence, explains the charge carrier manipulation observed through gated-PL as a signature of a highly-doping regime in semiconductors[19, 20, 25, 26, 31, 32].

In contrast, the t-BL18° gated-PL initially gives an impression that the system behaves as a semiconductor closer to the neutrality point in comparison to the t-BL1° device, in which the applied voltage barely promotes the appearance of trions in the emission response. It can be explained by considering that, although the **Q**-point also presents hybridized states, our DFT calculations reveal that the conduction and valence bands at the **K**-point are nearly degenerate and, thus, the system essentially behaves as two uncoupled MLs, further supporting the resemblance the PL spectra at RT of the ML case (see Figures 1d,f). The forming electrons may preferentially stay at **K**-point, promoting the excitonic formation mainly as an electron-hole pair at **K**-points at conduction and valence bands. RT gated-controlled PL supports those findings (Figures 2c,f,i) by showing no relevant changes when altering the charge carrier concentration (*n*- or *p*-type doping). One must note that inter-valley trions have been reported for TMD MLs[34–37]; however, mainly through external perturbation [36, 37] that alter the valley/or spin properties and, therefore, induce the formation of inter-valley trions. Here, we have shown that the stacking angle, on the other hand, can act as a charge-carrier controller as much as applied fields. It is worth mentioning that, although the  $\Gamma$ -point also presents the lowest energy point in the VB of t-BL1° and t-BL18°, inter-valley trions arising from electrons in **K**-point bounded to the holes in  $\Gamma$ - and **K**-points are not expected through the range of applied  $V_g$  due to the intrinsic *n*-doping character of our devices.

## CONCLUSION

In summary, this work investigates the optoelectronic properties of MoSe<sub>2</sub> homobilayers at room temperature through gated-PL spectroscopy. The experimental results showed an angle-alignment-dependent charge carrier concentration control, confirmed through small and large stacked-layer rotation samples. Combined with DFT calculations, our experimental results suggest that small twist angles favor the conduction band minima alteration at the **Q**-point, which promotes the photo-excited carriers to lie in **Q**-point, thus facilitating the formation of inter-valley trions. In contrast, a large-twist-angle mismatch provided a non-doped behaviour resembling the optical response of layered-decoupled monolayers. We also demonstrate that, even at room temperature, intralayer excitons may provide a trustworthy signature for the twist-angle vdWHs properties. Our findings significantly expanded the knowledge of TMD homobilayers by controlling their emission properties, which provides a fruitful groundwork for future potential applications of van der Waals semiconductor devices.

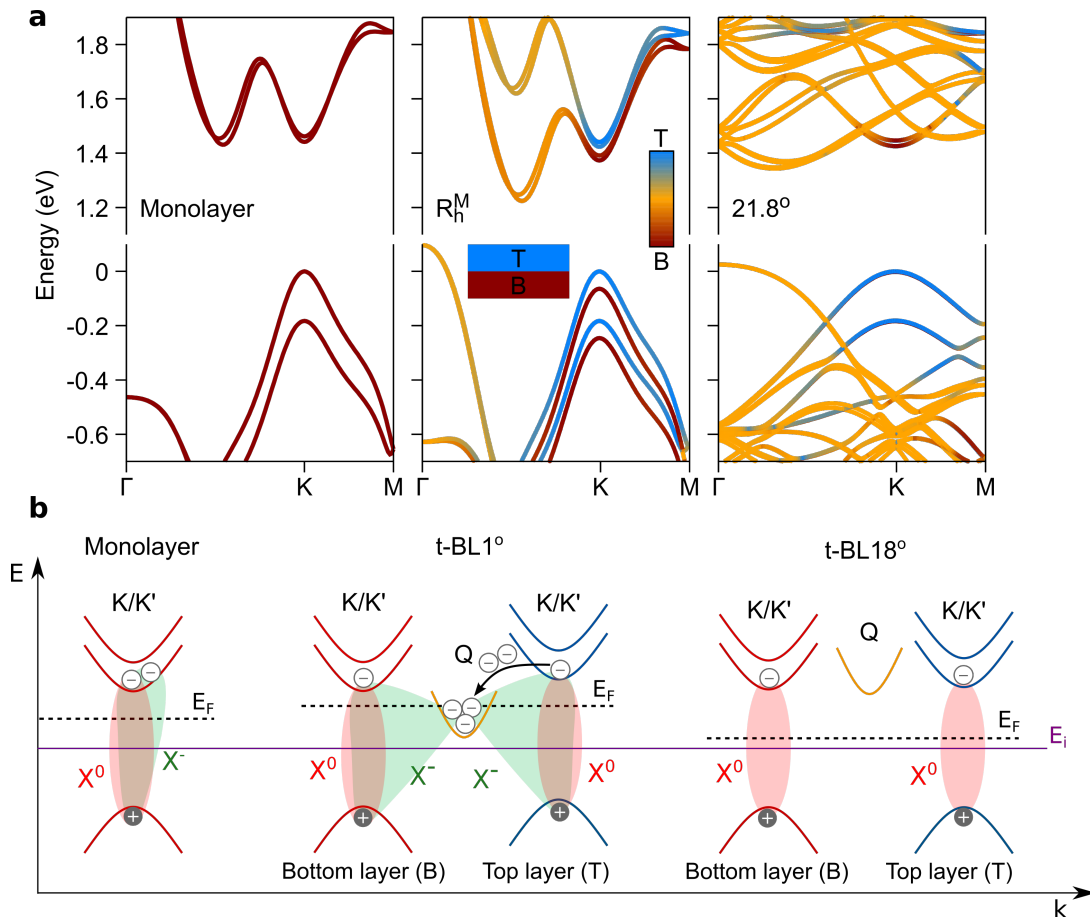


FIG. 3. **Band structure representation of MoSe<sub>2</sub> t-BLs devices.** (a) Calculated band structures for ML MoSe<sub>2</sub>,  $R_h^M$ -stacking bilayer MoSe<sub>2</sub>, and  $21.8^\circ$  twisted bilayer MoSe<sub>2</sub> along high-symmetry lines of the hexagonal first Brillouin zones. The color code represents the wave function localization throughout the top (T) and bottom (B) layers. For the  $21.8^\circ$  case, the conduction and valence bands near the **K** valleys are nearly degenerate, and the first Brillouin zone is smaller since the supercell has a lattice parameter of  $8.702 \text{ \AA}$ , nearly 2.65 times larger than the monolayer unit cell. (b) Schematic picture of the band structure and exciton complexes formation of a MoSe<sub>2</sub> ML, t-BL1° and t-BL18° under non-applied bias,  $V_g = 0$ .  $E_i$ ,  $E_F$ ,  $X^0$ , and  $X^-$  represent the intrinsic charge neutrality level, Fermi level, neutral exciton, and trion, respectively.

## METHODS

*Sample preparation.* The mechanical exfoliation[38] and the dry-transfer method[39] were performed through all 2D materials (MoSe<sub>2</sub> crystal, graphite (Gr) and hexagonal boron nitride (hBN)) used to fabricate our twisted MoSe<sub>2</sub> homobilayers. The MoSe<sub>2</sub> MLs were obtained by exfoliating TMD bulk crystals synthesized through flux zone growth [40] and identified by optical contrast and  $\mu$ PL spectroscopy. To create the t-BL devices, we used the tear-to-stack method [13]. The vdWHs composed by ( $\sim 10 \text{ nm}$ )hBN/MoSe<sub>2</sub>/MoSe<sub>2</sub>/( $\sim 20 \text{ nm}$ )hBN was transferred onto pre-selected few-layer Gr (FLG) flakes on a  $285 \text{ nm}$  SiO<sub>2</sub>/Si substrate. The devices were gated through electrical contacts made of Au(50 nm)/Cr(5 nm) patterned by electron-beam lithography and deposited using electron-beam evaporation.

*PL and gate-dependent PL measurements.*  $\mu$ PL measurements were performed at room and cryogenic (6 K) temperatures, the latter being carried out in a helium flow cryostat. In both conditions, the samples were excited non-resonantly using a CW 660 nm laser. Samples were excited, and the emission was collected through 50x and 20x long working distance objectives (NA=0.4), for the PL and PL-gate measurements, respectively. For the cryogenic measurements, the samples were placed in a He-flow cryostat. For PL-gated measurements, a pulse generator in combination with a source-meter was used. The PL emission was detected using a spectrometer equipped with thermoelectrically cooled charged-coupled device (CCD) (spectral resolution: 0.12 nm).

## SUPPLEMENTARY INFORMATION

Non-normalized gate-dependent PL for all devices, DFT calculation method, and supporting figures.

## CONFLICT OF INTEREST

The authors declare no competing financial interest.

## DATA AVAILABILITY STATEMENT

The data that support the findings of this study are available from the corresponding author upon reasonable request.

## ACKNOWLEDGEMENT

BLTR, YY, AKS, CCP and SR acknowledge financial support from the Deutsche Forschungsgemeinschaft (DFG, German Research Foundation) via projects Re2974/26-1 (within priority programm SPP 2244) and Re2974/21-1. PEFJ and JF acknowledge financial support of the DFG via SFB 1277 (Project-ID 314695032, projects B07 and B11), SPP 2244 (Project No. 443416183), and of the European Union Horizon 2020 Research and Innovation Program under Contract No. 881603 (Graphene Flagship). ARC acknowledges the financial support from the Brazilian Nanocarbon Institute of Science and Technology (INCT/Nanocarbono) and the National Council for Scientific and Technological Development (CNPq). The authors acknowledge Prof. Dr. Leandro Malard for enlightening discussion.

- 
- [1] Kyle L. Seyler, Pasqual Rivera, Hongyi Yu, Nathan P. Wilson, Essance L. Ray, David G. Mandrus, Jiaqiang Yan, Wang Yao, and Xiaodong Xu. Signatures of moiré-trapped valley excitons in MoSe<sub>2</sub>/WSe<sub>2</sub> heterobilayers. *Nature*, 567(7746):66–70, February 2019.
- [2] Evgeny M. Alexeev, David A. Ruiz-Tijerina, Mark Danovich, Matthew J. Hamer, Daniel J. Terry, Pramoda K. Nayak, Seongjoon Ahn, Sangyeon Pak, Juwon Lee, Jung Inn Sohn, Maciej R. Molas, Maciej Koperski, Kenji Watanabe, Takashi Taniguchi, Kostya S. Novoselov, Roman V. Gorbachev, Hyeon Suk Shin, Vladimir I. Fal’ko, and Alexander I. Tartakovskii. Resonantly hybridized excitons in moiré superlattices in van der waals heterostructures. *Nature*, 567(7746):81–86, March 2019.
- [3] Jiho Sung, You Zhou, Giovanni Scuri, Viktor Zólyomi, Trond I. Andersen, Hyobin Yoo, Dominik S. Wild, Andrew Y. Joe, Ryan J. Gelly, Hoseok Heo, Samuel J. Magorrian, Damien Bérubé, Andrés M. Mier Valdivia, Takashi Taniguchi, Kenji Watanabe, Mikhail D. Lukin, Philip Kim, Vladimir I. Fal’ko, and Hongkun Park. Broken mirror symmetry in excitonic response of reconstructed domains in twisted MoSe<sub>2</sub>/MoSe<sub>2</sub> bilayers. *Nature Nanotechnology*, 15(9):750–754, July 2020.
- [4] Trond I. Andersen, Giovanni Scuri, Andrey Sushko, Kristiaan De Greve, Jiho Sung, You Zhou, Dominik S. Wild, Ryan J. Gelly, Hoseok Heo, Damien Bérubé, Andrew Y. Joe, Luis A. Jauregui, Kenji Watanabe, Takashi Taniguchi, Philip Kim, Hongkun Park, and Mikhail D. Lukin. Excitons in a reconstructed moiré potential in twisted WSe<sub>2</sub>/WSe<sub>2</sub> homobilayers. *Nature Materials*, 20(4):480–487, January 2021.
- [5] Viviana Villafañe, Malte Kremser, Ruven Hübner, Marko M. Petrić, Nathan P. Wilson, Andreas V. Stier, Kai Müller, Matthias Florian, Alexander Steinhoff, and Jonathan J. Finley. Twist-dependent intra- and interlayer excitons in moiré homobilayers. *Physical Review Letters*, 130(2), January 2023.
- [6] Elizabeth Marcellina, Xue Liu, Zehua Hu, Antonio Fieramosca, Yuqing Huang, Wei Du, Sheng Liu, Jiixin Zhao, Kenji Watanabe, Takashi Taniguchi, and Qihua Xiong. Evidence for moiré trions in twisted MoSe<sub>2</sub> homobilayers. *Nano Letters*, 21(10):4461–4468, May 2021.
- [7] Frank Volmer, Manfred Ersfeld, Paulo E. Faria Junior, Lutz Waldecker, Bharti Parashar, Lars Rathmann, Sudipta Dubey, Iulia Cojocariu, Vitaliy Feyer, Kenji Watanabe, Takashi Taniguchi, Claus M. Schneider, Lukasz Plucinski, Christoph Stampfer, Jaroslav Fabian, and Bernd Beschoten. Twist angle dependent interlayer transfer of valley polarization from excitons to free charge carriers in WSe<sub>2</sub>/MoSe<sub>2</sub> heterobilayers. *npj 2D Materials and Applications*, 7(1), August 2023.
- [8] Weijie Li, Xin Lu, Sudipta Dubey, Luka Devenica, and Ajit Srivastava. Dipolar interactions between localized interlayer excitons in van der waals heterostructures. *Nature Materials*, 19(6):624–629, April 2020.
- [9] M. Van der Donck and F. M. Peeters. Interlayer excitons in transition metal dichalcogenide heterostructures. *Physical Review B*, 98:115104, Sep 2018.
- [10] Long Zhang, Zhe Zhang, Fengcheng Wu, Danqing Wang, Rahul Gogna, Shaocong Hou, Kenji Watanabe, Takashi Taniguchi, Krishnamurthy Kulkarni, Thomas Kuo, Stephen R. Forrest, and Hui Deng. Twist-angle dependence of moiré excitons in W<sub>2</sub>/MoSe<sub>2</sub> heterobilayers. *Nature Communications*, 11(1), November 2020.
- [11] Sebastian Meier, Yaroslav Zhumagulov, Matthias Dietl, Philipp Parzefall, Michael Kempf, Johannes Holler, Philipp Nagler, Paulo E. Faria Junior, Jaroslav Fabian, Tobias Korn, and Christian Schüller. Emergent trion-phonon coupling in atomically reconstructed mose<sub>2</sub>-wse<sub>2</sub> heterobilayers. *Phys. Rev. Res.*, 5:L032036, Sep 2023.
- [12] Bastian Miller, Alexander Steinhoff, Borja Pano, Julian Klein, Frank Jahnke, Alexander Holleitner, and Ursula Wurstbauer. Long-lived direct and indirect interlayer excitons in van der waals heterostructures. *Nano Letters*, 17(9):5229–5237, 2017. PMID: 28742367.
- [13] Kyoungwan Kim, Matthew Yankowitz, Babak Fallahzad, Sangwoo Kang, Hema C. P. Movva, Shengqiang Huang, Stefano Larentis, Chris M. Corbet, Takashi Taniguchi, Kenji Watanabe, Sanjay K. Banerjee, Brian J. LeRoy, and Emanuel Tutuc. van der waals heterostruc-



- tures with high accuracy rotational alignment. *Nano Letters*, 16(3):1989–1995, 2016. PMID: 26859527.
- [14] Yuan Cao, Valla Fatemi, Shiang Fang, Kenji Watanabe, Takashi Taniguchi, Efthimios Kaxiras, and Pablo Jarillo-Herrero. Unconventional superconductivity in magic-angle graphene superlattices. *Nature*, 556(7699):43–50, March 2018.
- [15] Philipp Tonndorf, Robert Schmidt, Philipp Boettger, Xiao Zhang, Janna Bierner, Andreas Liebig, Manfred Albrecht, Christian Kloc, Ovidiu Gordan, Dietrich R. T. Zahn, Steffen Michaelis de Vasconcellos, and Rudolf Bratschitsch. Photoluminescence emission and raman response of monolayer MoS<sub>2</sub>, MoSe<sub>2</sub> and We<sub>2</sub>. *Optics Express*, 21(4):4908, 2013.
- [16] Joshua O. Island, Agnieszka Kuc, Erik H. Diependaal, Rudolf Bratschitsch, Herre S. J. van der Zant, Thomas Heine, and Andres Castellanos-Gomez. Precise and reversible band gap tuning in single-layer MoSe<sub>2</sub> by uniaxial strain. *Nanoscale*, 8(5):2589–2593, 2016.
- [17] Kin Fai Mak, Keliang He, Changgu Lee, Gwan Hyoung Lee, James Hone, Tony F. Heinz, and Jie Shan. Tightly bound trions in monolayer MoS<sub>2</sub>. *Nature Materials*, 12(3):207–211, December 2012.
- [18] Sergii Golovynskiy, Oleksandr I. Datsenko, Dan Dong, Yan Lin, Iqra Irfan, Baikui Li, Danying Lin, and Junle Qu. Trion binding energy variation on photoluminescence excitation energy and power during direct to indirect bandgap crossover in monolayer and few-layer MoS<sub>2</sub>. *The Journal of Physical Chemistry C*, 125(32):17806–17819, August 2021.
- [19] Jingzhi Shang, Xiaonan Shen, Chunxiao Cong, Namphung Peimyoo, Bingchen Cao, Mustafa Eginligil, and Ting Yu. Observation of excitonic fine structure in a 2d transition-metal dichalcogenide semiconductor. *ACS Nano*, 9(1):647–655, 2015. PMID: 25560634.
- [20] Bairen Zhu, Xi Chen, and Xiaodong Cui. Exciton binding energy of monolayer WS<sub>2</sub>. *Scientific Reports*, 5(1), 2015.
- [21] Matthias Drüppel, Thorsten Deilmann, Peter Krüger, and Michael Rohlfing. Diversity of trion states and substrate effects in the optical properties of an MoS<sub>2</sub> monolayer. *Nature Communications*, 8(1), December 2017.
- [22] Yeongsu Cho and Timothy C. Berkelbach. Environmentally sensitive theory of electronic and optical transitions in atomically thin semiconductors. *Phys. Rev. B*, 97:041409, Jan 2018.
- [23] Chirag Chandrakant Palekar, Joakim Hagel, Barbara Rosa, Samuel Brem, Ching-Wen Shih, Imad Limame, Martin von Helversen, Sefaattin Tongay, Ermin Malic, and Stephan Reitzenstein. Anomalous redshift in interlayer exciton emission with increasing twist angle in wse<sub>2</sub>/mose<sub>2</sub> heterostructures. *2D Materials*, 11(2):025034, March 2024.
- [24] Der-Hsien Lien, Shiekh Zia Uddin, Matthew Yeh, Matin Amani, Hyungjin Kim, Joel W. Ager, Eli Yablonovitch, and Ali Javey. Electrical suppression of all nonradiative recombination pathways in monolayer semiconductors. *Science*, 364(6439):468–471, May 2019.
- [25] Alisson Cadore, Bárbara Luiza Teixeira Rosa, Ioannis Paradisanos, Sandro Mignuzzi, Domenico De Fazio, Eugene Alexeev, Alva Dagkli, Jakob Muench, Georgios Kakavelakis, Sachin M. Schinde, Duhee Yoon, Sefaattin Tongay, Kenji Watanabe, Takashi Taniguchi, Eleftherios Lidorikis, Ilya Goykhman, Giancarlo Soavi, and Andrea C Ferrari. Monolayer WS<sub>2</sub> electro- and photoluminescence enhancement by tfsi treatment. *2D Materials*, 11:025017, January 2024.
- [26] S. M. Sze. *Semiconductor devices: physics and technology / S.M. Sze*. Wiley, New York, 2nd ed. edition, 2002.
- [27] Gerd Plechinger, Philipp Nagler, Ashish Arora, Robert Schmidt, Alexey Chernikov, Andrés Granados del Águila, Peter C.M. Christianen, Rudolf Bratschitsch, Christian Schüller, and Tobias Korn. Trion fine structure and coupled spin–valley dynamics in monolayer tungsten disulfide. *Nature Communications*, 7(1), September 2016.
- [28] Jason S. Ross, Sanfeng Wu, Hongyi Yu, Nirmal J. Ghimire, Aaron M. Jones, Grant Aivazian, Jiaqiang Yan, David G. Mandrus, Di Xiao, Wang Yao, and Xiaodong Xu. Electrical control of neutral and charged excitons in a monolayer semiconductor. *Nature Communications*, 4(1), February 2013.
- [29] A M Stoneham. Non-radiative transitions in semiconductors. *Reports on Progress in Physics*, 44(12):1251–1295, December 1981.
- [30] Yuze Meng, Tianmeng Wang, Chenhao Jin, Zhipeng Li, Shengnan Miao, Zhen Lian, Takashi Taniguchi, Kenji Watanabe, Fengqi Song, and Su-Fei Shi. Electrical switching between exciton dissociation to exciton funneling in MoSe<sub>2</sub>/W<sub>2</sub> heterostructure. *Nature Communications*, 11(1), May 2020.
- [31] Shunfeng Wang, Junyong Wang, Weijie Zhao, Francesco Giustiniano, Lei qiang Chu, Ivan Verzhbitskiy, Justin Zhou Yong, and Goki Eda. Efficient carrier-to-exciton conversion in field emission tunnel diodes based on mis-type van der waals heterostack. *Nano Letters*, 17(8):5156–5162, July 2017.
- [32] Dohyun Kwak, Matthias Paur, Kenji Watanabe, Takashi Taniguchi, and Thomas Mueller. High-speed electroluminescence modulation in monolayer WS<sub>2</sub>. *Advanced Materials Technologies*, 7(5), October 2021.
- [33] Paulo E. Faria Junior and Jaroslav Fabian. Signatures of electric field and layer separation effects on the spin-valley physics of MoSe<sub>2</sub>/We<sub>2</sub> heterobilayers: From energy bands to dipolar excitons. *Nanomaterials*, 13(7), 2023.
- [34] T. P. Lyons, S. Dufferwiel, M. Brooks, F. Withers, T. Taniguchi, K. Watanabe, K. S. Novoselov, G. Burkard, and A. I. Tartakovskii. The valley zeeman effect in inter- and intra-valley trions in monolayer wse<sub>2</sub>. *Nature Communications*, 10(1), May 2019.
- [35] F. Volmer, S. Pissinger, M. Ersfeld, S. Kuhlen, C. Stampfer, and B. Beschoten. Intervalley dark trion states with spin lifetimes of 150 ns in wse<sub>2</sub>. *Physical Review B*, 95:235408, Jun 2017.
- [36] Yan Zhang, Keisuke Shinokita, Kenji Watanabe, Takashi Taniguchi, Yuhei Miyauchi, and Kazunari Matsuda. Magnetic field induced inter-valley trion dynamics in monolayer 2d semiconductor. *Advanced Functional Materials*, 31(4), October 2020.
- [37] Jiajie Pei, Xue Liu, Andrés Granados del Águila, Di Bao, Sheng Liu, Mohamed-Raouf Amara, Weijie Zhao, Feng Zhang, Congya You, Yongzhe Zhang, Kenji Watanabe, Takashi Taniguchi, Han Zhang, and Qihua Xiong. Switching of k-q intervalley trions fine structure and their dynamics in n-doped monolayer WS<sub>2</sub>. *Opto-Electronic Advances*, 6(4):220034–220034, 2023.
- [38] K. S. Novoselov, A. K. Geim, S. V. Morozov, D. Jiang, Y. Zhang, S. V. Dubonos, I. V. Grigorieva, and A. A.



- Firsov. Electric field effect in atomically thin carbon films. *Science*, 306(5696):666–669, October 2004.
- [39] Andres Castellanos-Gomez, Michele Buscema, Rianda Molenaar, Vibhor Singh, Laurens Janssen, Herre S J van der Zant, and Gary A Steele. Deterministic transfer of two-dimensional materials by all-dry viscoelastic stamping. *2D Materials*, 1(1):011002, April 2014.
- [40] Masanori Nagao. Crystal growth techniques for layered superconductors. *Condensed Matter*, 2(4):32, October 2017.